*SF2A 2019*
*P. Di Matteo, O. Creevey, A. Crida, G. Kordopatis, J. Malzac, J.-B. Marquette, M. N'Diaye, O. Venot (eds)*

# 3D MAGNETO-HYDRODYNAMIC SIMULATIONS TO COUNTERACT THE CONVECTIVE NOISE SOURCE FOR EXTRASOLAR PLANET DETECTION

S. Sulis[1,2], L. Bigot[2] and D. Mary[2]

**Abstract.** Convection transports energy from the stellar interior towards the surface in late type stars. Its properties are essential to understand the stellar structure and evolution and can now be reliably inferred by modern 3D magneto-hydrodynamic simulations. Convection is also a significant noise source for detecting extrasolar planets. In this paper, we analyze the potential of 3D MHD simulations in reproducing realistic time series of radial velocity to estimate the statistical properties of this noise source and, in turn, to improve exoplanets' detectability.

Keywords: Sun: granulation, Techniques: radial velocities, Planets and satellites: detection

## 1 Introduction

Resolved observations of the Sun clearly show moving granular structures that are the manifestation of the convection at the solar photosphere. Present at the surface of all late type stars, convection transports energy from the stellar interior towards the surface and is a key process to understand the stellar structure and evolution. Indeed, the dynamics of the convective cells define the thermal stellar stratification, mix the chemical elements and generate the surface acoustics modes.
Since the 90's, 3D magneto-hydrodynamic simulations (MHD) are developed (Nordlund & Galsgaard 1995) based on radiative compressive hydrodynamics equations (including the wavelength-dependent radiative transfer) as well as on realistic equations-of-state that accounts for ionization, recombination, dissociation (Mihalas et al. 1988) and line opacity (Gustafsson et al. 2008). Generally used for stellar diagnostics (e.g. chemical abundances, limb darkenings, radial velocities), they succeed in reproducing the properties of the stellar convection (granules' size, lifetime, spectral lines shape).
For late-type stars others than the Sun, convection is not resolved but its properties are extracted indirectly from variations of the spectroscopic stellar lines and the photometric variability in integrated starlight (Dravins & Lind 1984). While the study of these different signatures informs a lot on the star, this variability represents a significant noise source hampering the detection of smaller stellar (e.g. acoustic and gravity modes) and planetary signals.
From solar observations, we know that granulation can generate variability with amplitudes up to several tenth of centimeters per second in radial velocities (RV) (Saar & Donahue 1997). This is significant compared to the signal from Earth-like planets : we expect that a Earth orbiting a Sun generate a RV signal of 9 $cm.s^{-1}$ amplitude only (Wright 2018). Thus, the signatures of stellar granulation need to be understood and "statistically controlled" to be able to reliably detect Earth-analogues (Meunier et al. 2015). In Sulis et al. (2017), we demonstrated that using synthetic time series of a granulation noise leads to a better control of the detection tests statistics. We focus in the present paper on the possibility of using MHD simulations to reproduce convection noise of a specific star, the Sun, and we illustrate how the approach can improve the detection of low mass extrasolar planets by the RV technique.

[1] Space Research Institute, Austrian Academy of Sciences, Schmiedlstraße 6, 8042 Graz, Austria
[2] Université Côte d'Azur, Observatoire de la Côte d'Azur, CNRS, Lagrange UMR 7293, CS 34229, 06304, Nice Cedex 4, France

## 2 Simulations of the solar granulation

Modern MHD codes simulate the surface convection and its stratification over the stellar photosphere in 3D cartesian-box (Nordlund 1985). In this study, we use the STAGGER CODE*, described in Nordlund & Galsgaard (1995) that simulates granulation in a box of size $8000 \times 8000$ kms and $+500$ and $-3400$ km above and below the surface at optical depth $\tau = 1$. The code solves the full set of conservative hydrodynamical equations coupled to an accurate treatment of the radiative transfer. The solar parameters that define our 3D model are $T_{\rm eff} = 5775 \pm 30$ K, $\log g = 4.44$ and a solar chemical composition (Asplund et al. 1999). We impose a traverse magnetic field at the bottom of the simulation's boxes so that the averaged surface field is roughly 100 G, as observed with spectropolarimetry (Trujillo Bueno et al. 2004). The detailed description of this simulation will be published in an article currently in preparation. In total, we generate the evolution of 76 528 snapshots of solar convection corresponding to 53.14 days of physical time (with a temporal sampling of 60 seconds). This is, to our knowledge, the longest simulated time series of granulation ever generated with such a 3D code.

This kind of 3D simulations have already shown their accuracy in resolving observations of the solar surface, see e.g. similarities of the observed structures in continuum intensities (Danilovic et al. 2008) or of the spectrally resolved solar lines width and asymmetries (Asplund et al. 2000). However, their efficiency in retrieving the disk integrated RV properties is still unproved. One reason is that the 3D simulations are too computationally time consuming to simulate what would be the contribution of thousands of convection boxes covering the entire solar disk. In the following subsections, we discuss the influence of the size of the simulated patch as well as its position on the resulting line-of-sight velocities, and present a first comparison of disk-integrated velocities with solar spatial observations.

### *2.1 3D local simulation patch: velocity dependence on the surface size area*

To illustrate the dependence of the observed velocities with the size of the considered surface area, we selected different sizes of solar images taken by the *Helioseismic and Magnetic Imager* (HMI) on board the *Solar Dynamics Observatory* (SDO; Schou et al. (2012)). Fig. 1 shows the RV extracted from these solar images. We see the decrease of the velocity amplitudes with the size of the observed surface of the solar disk. Quantitatively, the velocity root-mean-square (rms) corresponding to a single granule, a set of tenth granules, a single supergranule and a set of tenth supergranules are 247.2, 105.2, 12.3, and 2.3 m.s$^{-1}$, respectively. This decrease in amplitude is due to a cancellation effect between the contribution of the upflows in the granules' center and the downflows in the intergranular lanes. When comparing this size-dependent observations to the simulated velocity extracted from 3D boxes of similar sizes, we observe a consistent decrease in amplitude. This is shown in the second and last panel of Fig. 1 using 3D simulations of supergranulation (R. Stein, priv. communication) and granulation†.

*`http://www.astro.ku.dk/~kg/Papers/MHDcode.ps.gz`

†In this figure, the granulation velocity has been extracted by considering a subset of the supergranulation 3D box.

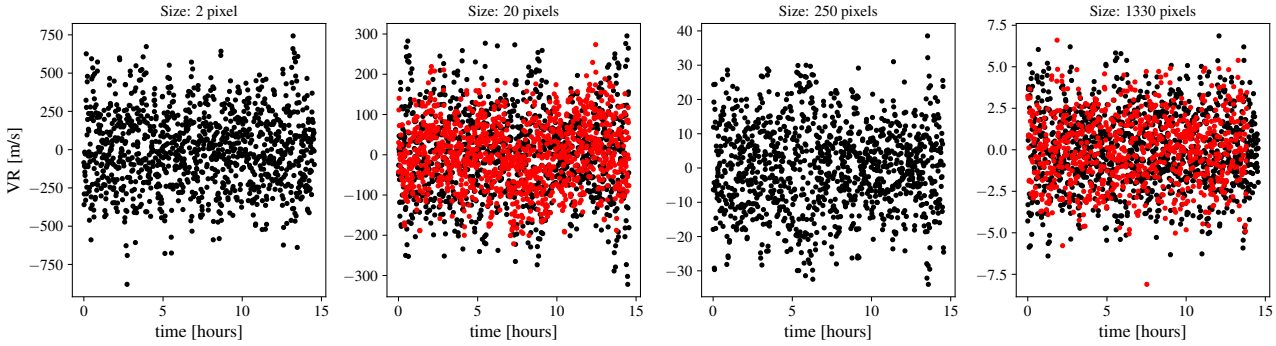


**Fig. 1.** Sequence of solar radial velocities extracted from HMI/SDO observations (black) for different sizes of the solar surface (in pixel). The size is indicated in the panels' title with 1 pixel corresponding to $\approx 388$ km. From left to right the size corresponds roughly to the size of a granule, the size covered by a 3D cartesian-box of granulation, the size of a supergranule and the size covered by a 3D cartesian-box of supergranulation. Synthetic velocities extracted from 3D MHD simulations are compared with observations in the second and last panels (red).

### 2.2 Inclination of the 3D patch: velocities from center to limb

The line-of-sight projected velocity depends also on the relative distance of the observed surface to the disk center. At a given time, this velocity can be decomposed as a combination of a radial and an horizontal component. The horizontal component, higher in amplitude, is completely cancelled out by projection effect when we look at the center of the solar disk ($\mu = \cos\theta = 1$). At limb, however, the vertical flow vanishes and only the horizontal component contributes to the line-of-sight velocity (Nordlund et al. 2009). The resulting decrease of the velocity amplitudes observed from the limb to the center of the disk is shown in Fig. 2. Hence, the resulting velocities depend critically on the exact region of the solar surface that is observed (Löhner-Böttcher et al. 2018). These amplitudes also depend on the properties of the considered spectral line and on the strength of the local magnetic field as shown in Cegla et al. (2018). Once integrated over the limb angle, the horizontal component is compensated by the radial flows of the disk center. This leads to RV time series of several tenths of cm.s$^{-1}$ in amplitude – which is still enough to mimic/hide RV signatures of small exoplanets.

### 2.3 Disk-integrated velocities

To compare the simulated velocities with disk-integrated solar observations, we selected observations taken from space by the *Global Oscillation at Low Frequencies* (GOLF) resonant scattering spectrophotometer on board the *Solar and Heliospheric Observatory* (SoHO; Gabriel et al. (1995)). GOLF provides continuous measurements of the sodium doublet lines at $\lambda = 5895.924$ Å and 5889.950 Å . The data, calibrated by Appourchaux et al. (2018), consist in 22 years of almost continuous observations regularly sampled every 20 seconds.
To reproduce these observations, we computed synthetic spectra of the sodium doublet for different $\mu$ cosine angles. We then covered the solar surface with simulation patches taken at different time, and we associated to each of them the $\mu$ angle corresponding to the patch position on the disk. We integrated the resulting flux to obtain the global disk-integrated velocity at a given time. The detailed description of this procedure will be given in a forthcoming paper.

The final comparison between observed and calibrated disk-integrated synthetic velocities of the solar granulation is shown in panels (a) and (b) of Fig. 3 for the periodograms and velocities, respectively. We observe a good match between the power spectrum density (PSD) estimates over the correlation regime dominated by the granulation noise (i.e., for $\nu$ typically in the range $[30, 1000]$ $\mu$Hz).

## 3 Design of powerful detection tests

As studied in Sulis et al. (2017), simulations of granulation noise can be exploited to calibrate (or standardize) the periodogram of the observations in order to design more reliable detection tests. In fact, in the case of regularly sampled observations, the distribution of the resulting standardized periodogram ($\widetilde{P}$, see Eq. (8) of Sulis et al. (2017)) is essentially independent of the granulation noise PSD under the null hypothesis $\mathcal{H}_0$ (i.e., when only noise is present in the data). Hence, the false alarm probability ($P_{FA}$) is *independent of the considered star's granulation*. This is a very interesting feature in practice, which is not present for tests based on the classical periodogram ($P$). The test threshold can be used to control the $P_{FA}$ in the case of $\widetilde{P}$ but not of $P$, because in the latter case the distribution of the considered detection test depends on the unknown PSD of the granulation noise.

We now wish to investigate, on a real data set from GOLF, the agreement between our theoretical results

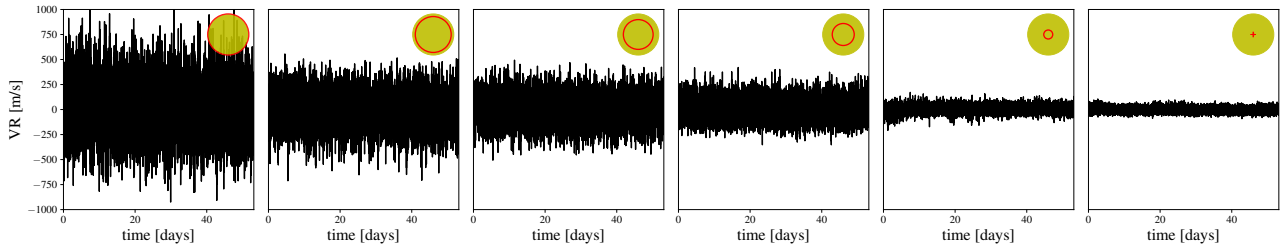


**Fig. 2.** Simulated velocities for different center to limb cosine angles ($\mu$). From left to right: $\mu = 0.12$, 0.39, 0.60, 0.80, 0.92, 1.00. On each panel, the red circle illustrates the considered $\mu$-isocontour.

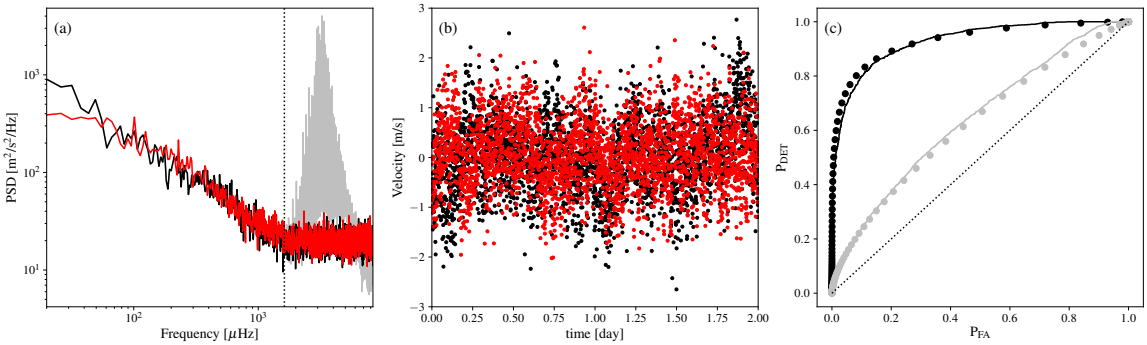


**Fig. 3.** (a-b) Comparison between GOLF observations (black) and synthetic RV generated using 3D codes (red). Oscillation modes and high frequencies ($\nu_c > 1620$ $\mu$Hz, see the vertical dotted line in (b)) have been filtered out (in gray : periodogram of synthetic RV with p-modes not filtered out). To restore the flat, high frequency part of GOLF data, we added a white Gaussian noise with variance estimated using GOLF raw periodogram (at frequencies $\nu > \nu_c$). (c) Empirical (solid) and theoretical (dots) ROC curves of tests $T_M(\widetilde{P})$ for planets with mass $\mathrm{M_p} = 0.25$ $\mathrm{M_\oplus}$ (black) and $\mathrm{M_p} = 0.15$ $\mathrm{M_\oplus}$ (gray) under $\mathcal{H}_1$.

and the actual performances of a particular detection test. The periodogram of GOLF data is here standardized by synthetic velocities coming from our MHD simulations. Consider the test of the maximum periodogram value (see Sulis et al. (2017) for several other interesting tests and their comparison), whose test statistic is defined as $T_M(\widetilde{P}) := \max_{\nu} \widetilde{P}(\nu)$. This test claims a detection if the highest peak of $\widetilde{P}$ is above a predefined threshold. On the theoretical front, analytical expressions for the $P_{DET}$ and the $P_{FA}$ as a function of the number of available noise time series are derived in Chap 3. (Eq. (3.18) and (3.19)) of Sulis (2017). Here, we compare these theoretical expressions with empirical results derived using solar observations. For this comparison, we selected as a data set under $\mathcal{H}_0$ a batch of 1679 sequences of regularly sampled ($dt = 1$ minute) 2-day length solar time series ($N = 2880$ data points for each time series). To build a data set with planetary signals in the considered frequency range[‡], we added to each of these sequences the RV signature of a planet, with 0.25 and 0.15 Earth mass ($M_\oplus$)[§] We then computed the empirical probability of detection ($P_{DET}$) and the $P_{FA}$ for the test $T_M(\widetilde{P})$ with $\widetilde{P}$ the periodogram of GOLF observations standardized by an averaged periodogram coming from the average of $L = 20$ synthetic RV time series generated through our MHD simulations. The resulting empirical *Receiver Operating Characteristic* (ROC) curves, that represent the $P_{DET}$ as a function of the $P_{FA}$, are shown in Fig. 3, panel (c). Logically, the performances of both tests increase with the planet's mass. Comparing now the theoretical and empirical ROCs curves of the test for a given mass and a given $P_{FA}$, we observe a good match of the curves in both cases. This shows that the MHD based approach is successful in controlling, theoretically and in practice, the statistical performance of the test, although the PSD of the granulation noise is partially unknown.

## 4 Conclusions

Reliably detecting low mass planets whose signatures are buried in the stellar noise is a difficult point. Based on GOLF data, our results show that for Solar-like stars, 3D MHD simulations can be used to generate realistic RV synthetic time series of the granulation noise. These simulations can further be used as training data sets to control accurately the false alarm rate of detection tests in presence of granulation noise.

S. Sulis acknowledges support from the Austrian Research Promotion Agency (FFG) under project 859724 "GRAPPA". We acknowledge financial support from "Programme National de Physique Stellaire" (PNPS) of CNRS/INSU, CEA and CNES, France

[‡]To avoid the influence of other noise sources, we considered only frequencies $\nu \in [30, 1000]$ $\mu$Hz.
[§]The other Keplerian parameters are fixed: period= 4 hours, inclination and argument of periapsis = $\pi/2$ rad, eccentricity= 0.

## References

Appourchaux, T., Boumier, P., Leibacher, J. W., & Corbard, T. 2018, A&A, 617, A108
Asplund, M., Nordlund, Å., Trampedach, R., Allende Prieto, C., & Stein, R. F. 2000, A&A, 359, 729
Asplund, M. et al. 1999, A&A, 346, L17
Cegla, H. M., Watson, C. A., Shelyag, S., et al. 2018, ApJ, 866, 55
Danilovic, S., Gandorfer, A., Lagg, A., et al. 2008, A&A, 484, L17
Dravins, D. & Lind, J. 1984, in Small-Scale Dynamical Processes in Quiet Stellar Atmospheres, ed. S. L. Keil, 414
Gabriel, A. H. et al. 1995, Solar Physics, 162, 61
Gustafsson, B., Edvardsson, B., Eriksson, K., et al. 2008, A&A, 486, 951
Löhner-Böttcher, J., Schmidt, W., Stief, F., Steinmetz, T., & Holzwarth, R. 2018, A&A, 611, A4
Meunier, N. et al. 2015, A&A, 583, A118
Mihalas, D., Dappen, W., & Hummer, D. G. 1988, ApJ, 331, 815
Nordlund, Å. 1985, Solar Physics, 100, 209
Nordlund, Å. & Galsgaard, K. 1995, Technical report, Astronomical Observatory, Copenhagen University,
Nordlund, Å. et al. 2009, Living Reviews in Solar Physics, 6, 2
Saar, S. H. & Donahue, R. A. 1997, The Astrophysical Journal, 485, 319
Schou, J., Scherrer, P. H., Bush, R. I., et al. 2012, Sol. Phys., 275, 229
Sulis, S. 2017, PhD thesis, supervised by par Mary, D. and Bigot, L., Université Côte d'Azur 2017, `http://www.theses.fr/2017AZUR4073/document`
Sulis, S., Mary, D., & Bigot, L. 2017, IEEE TSP, 65, 2136
Trujillo Bueno, J., Shchukina, N., & Asensio Ramos, A. 2004, Nature, 430, 326
Wright, J. T. 2018, Radial Velocities as an Exoplanet Discovery Method, 4